Characterization of the Interacting Domain of the HIV-1 Fusion Peptide with the Transmembrane Domain of the T-Cell Receptor†

Tomer Cohen,‡ Meirav Pevsner-Fischer,§ Noam Cohen,§ Irun R. Cohen,§ and Yechiel Shai*,‡

Departments of Biological Chemistry and Immunology, the Weizmann Institute of Science, Rehovot 76100, Israel

Received January 18, 2008; Revised Manuscript Received February 26, 2008

ABSTRACT: HIV infection is initiated by the fusion of the viral membrane with the target T-cell membrane. The HIV envelope glycoprotein, gp41, contains a fusion peptide (FP) in the N terminus that functions together with other gp41 domains to fuse the virion with the host cell membrane. We recently reported that FP co-localizes with CD4 and T-cell receptor (TCR) molecules, co-precipitates with TCR, and inhibits antigen-specific T-cell proliferation and pro-inflammatory cytokine secretion. Molecular dynamic simulation implicated an interaction between an α-helical transmembrane domain (TM) of the TCRα chain (designated CP) and the β-sheet 5–13 region of the 16 N-terminal amino acids of FP ($FP_{1–16}$). To correlate between the theoretical prediction and experimental data, we synthesized a series of mutants derived from the interacting motif GALFLGFLG stretch ($FP_{5–13}$) and investigated them structurally and functionally. The data reveal a direct correlation between the β-sheet structure of $FP_{5–13}$ and its mutants and their ability to interact with CP and induce immunosuppressive activity; the phenylalanines play an important role. Furthermore, studies with fluorescently labeled peptides revealed that this interaction leads to penetration of the N terminus of FP and its active analogues into the hydrophobic core of the membrane. A detailed understanding of the molecular interactions mediating the immunosuppressive activity of the $FP_{5–13}$ motif should facilitate evaluating its contribution to HIV pathology and its exploitation as an immunotherapeutic tool.

Enveloped viruses require a fusion of the viral membrane with the cellular membrane in the initial step of infection. The process of fusing the HIV membrane with the target T-cell membrane is catalyzed by the HIV glycoprotein gp41, which comprises several functional domains that contribute to the fusion process (*1–5*). Among them, the 33 residues at the N terminus (the fusion peptide, $FP_{1–33}$) is of great importance (*1, 3, 6–10*) (Figure 1). Two different domains were identified within $FP_{1–33}$: the 16 amino acid long hydrophobic stretch ($FP_{1–16}$) in the N terminus that inserts into the host cell membrane and the C-terminus hydrophilic region that lies parallel to the cell surface (*11–14*).

During the initial step of the membrane fusion process, $FP_{1–16}$ anchors gp41 to the target membrane. In the next step, conformational changes of gp41 bridge the gap between the opposing membranes and eventually complete the fusion process (*5, 15–17*). In an attempt to better understand the interaction of FP with T-cell membranes, we synthesized peptides that resemble or mimic the regions of the putative fusion peptide and investigated their interaction with T cells (*18*). The data revealed that FP co-localizes with CD4 and TCR molecules and co-precipitates with T-cell receptor α subunit (TCRα).[1] This interaction inhibits antigen-specific T-cell proliferation and pro-inflammatory cytokine secretion *in vitro*, leading to T-cell immunosuppression, which might function to suppress the HIV-specific immunity. In addition, it facilitates the spread of HIV to uninfected cells (*18*). We have also shown that this immunosuppressive activity of FP

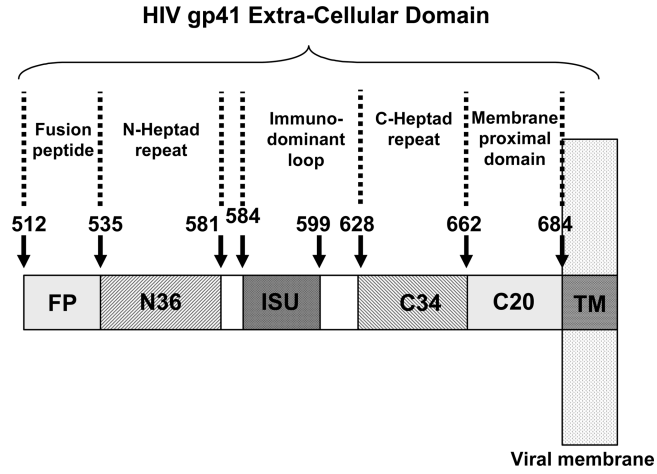

FIGURE 1: HIV-1 gp41 extracellular domain. A cartoon showing functional regions within the extracellular portion of gp41 (amino acids 512–684).

† This study was supported by the Israel Science Foundation to Y.S.

* To whom correspondence should be addressed: Department of Biological Chemistry, the Weizmann Institute of Science, Rehovot, 76100 Israel. Telephone: 972-8-9342712. Fax: 972-9344112. E-mail: yechiel.shai@weizmann.ac.il.

‡ Department of Biological Chemistry.

§ Department of Immunology.

[1] Abbreviations: ATR−FTIR, attenuated total reflectance Fourier transform infrared; CP, core peptide; FP, fusion peptide; LUV, large unilamellar vesicle; PC, phosphatidylcholine; TM, transmembrane; TCRα, T-cell receptor α subunit; RP-HPLC, reverse-phase high-performance liquid chromatography.

10.1021/bi800100p CCC: $40.75
Published on Web 04/01/2008

Table 1: Designations and Sequences of the Peptides Investigated in This Study[a]

designation	sequence
$FP_{1–16}$	A V G I G A L F L G F L G A A G
$FP_{5–13}$	G A L F L G F L G
$FP_{5–13}$ FFxGG	G A L **G** L G **G** L G
$FP_{5–13}$ LLxGG	G A L F **G** G F **G** G
$FP_{5–13}$ FFxVV	G A L **V** L G **V** L G
$FP_{5–13}$ LLxVV	G A L F **V** G F **V** G
$FP_{5–13}$ AAAA	G A L **A** **A** G **A** **A** G
CP[b]	G L R I L L L K V

[a] Substituted amino acids are in bold and underlined. [b] The sequence of CP was taken from Manolios and co-workers (*56*).

could be exploited as an immunotherapeutic tool by reducing the clinical signs of the experimental autoimmune T-cell-mediated disease adjuvant arthritis (AA) (*18*).

The contribution of the different regions of FP to membrane fusion has been previously well-characterized (*1, 5, 19–22*). However, their role in the immunosuppressive activity of FP is still unknown. Recently, we used molecular dynamic simulation to identify the TCR/$FP_{1–33}$ interaction motif at the molecular level, providing a 3D model of the TCR/FP complex structure, and reported that the $FP_{5–13}$ region might play a role in the TCR/FP interaction (*23*).

In this study, we examined the contribution of the amino acids and the structural requirements of this highly conserved and hydrophobic GALFLGFLG stretch ($FP_{5–13}$) by synthesizing and investigating its mutants (Table 1). Our data reveal that the $FP_{5–13}$ region is a conserved motif, in which phenylalanines significantly contribute to its function and β-sheet conformation. This structure is important for the interaction with TCRα TM (designated here CP) to induce immunosuppressive activity. Importantly, a similar β-sheet structure has also been implicated as the fusion-active conformation of FP under similar conditions. Note however that previous structural characterization of the FP has revealed contradictory data; α helix or β structure (*3, 6, 8, 9, 14, 24–39*). This apparent dichotomy may be explained by structural plasticity, which serves a specific purpose during the fusion process. The α-helical structure is more stabilized at low peptide/lipid molar ratios, whereas the β-sheet structure was implicated at higher peptide/lipid molar ratios. A detailed understanding of the molecular interactions mediating the immunosuppressive activity of the $FP_{5–13}$ motif should facilitate the evaluation of its contribution to HIV pathology and its exploitation as an immunotherapeutic tool.

EXPERIMENTAL PROCEDURES

Materials. Rink amide MBHA resin and 9-fluorenylmethoxycarbonyl (Fmoc) amino acids were purchased from Calibochem-Novabiochem AG (Switzerland). Other reagents used for peptide synthesis include *N*,*N*-diisopropylethylamine (DIEA, Aldrich), dimethylformamide, dicheloromethane, and piperidine (Biolab, IL). Egg phosphatidylcholine (PC) was purchased from Lipid Products (South Nutfield, U.K.). 4-Chloro-7-nitrobenz-2-oxa-1,3-diazole fluoride (NBD-F) was purchased from Molecular Probes (Junction City, OR). The myelin oligodendrocyte glycoprotein (MOG) p35-55 antigen used for the specific activation of the T-cell line was synthesized using the F-MOC technique with an automatic multiple peptide synthesizer (AMS 422, ABIMED, Langenfeld, Germany). The Hamster antimouse anti-CD3 antibody was collected by trichloroacetic acid (TCA) precipitation from 2C11 hybridoma supernatant.

Peptide Synthesis and Fluorescent Labeling. Peptides were synthesized using the F-moc solid-phase method on Rink amide resin (0.68 mequiv), as previously described (*10*). The synthetic peptides were purified (greater than 98% homogeneity) by reverse-phase high-performance liquid chromatography (RP-HPLC) on a C4 column using a linear gradient of 30–70% acetonitrile in 0.1% trifluoroacetic acid (TFA) for 40 min. The peptides were subjected to amino acid and mass spectrometry analysis to confirm their composition. To avoid aggregation of the peptides prior to their use in the cell-culture assays, the stock solutions of the concentrated peptides were maintained in dimethyl sulfoxide (DMSO). The final concentration of DMSO in each experiment was lower than 0.25% (vol/vol) and had no effect on the system under investigation. For fluorescent labeling, resin-bound peptides were treated with NBD-F (2-fold excess) dissolved in dimethyl formamide (DMF), leading to the formation of resin-bound N-terminal NBD peptides (*40*). After 1 h, the resins were washed thoroughly with DMF and then with methylene chloride, dried under nitrogen flow, and then cleaved for 3 h with 95% TFA, 2.5% H_2O, and 2.5% triethylsilane. The labeled peptides were purified on a RP-HPLC C4 column as described above. Unless stated otherwise, stock solutions of concentrated peptides were maintained in DMSO to avoid aggregation of the peptides prior to use.

Attenuated Total Reflectance Fourier Transform Infrared (ATR−FTIR) Spectroscopy. Spectra were obtained with a Bruker equinox 55 FTIR spectrometer equipped with a deuterated triglyceride sulfate (DTGS) detector, coupled with an ATR device. For each spectrum, 150 scans were collected, with a resolution of 4 cm^{-1}. Samples were prepared as described (*41*). Briefly, lipids alone or with a peptide were deposited on a ZnSe horizontal ATR prism (80 × 7 mm). Before the sample was prepared, the trifluoroacetate (CF_3COO^-) counterions, which strongly associate with the peptide, were replaced by chloride ions through several washings in 0.1 M HCl and lyophilization. This eliminated the strong C═O stretching absorption band near 1673 cm^{-1} (*42*). Peptides were dissolved in MeOH, which was chosen over DMSO, used in the lipid mixing experiments, because MeOH evaporates readily and is a suitable solvent for the lipids. Lipids were dissolved in a 1:2 MeOH/$CHCl_3$ mixture. Lipid−peptide mixtures at a 200:1 molar ratio or lipids alone with the corresponding volume of methanol were spread with a Teflon bar on the ZnSe prism. The solvents were eliminated by drying under vacuum for 15 min. Pure phospholipid spectra were subtracted to yield the difference spectra. The background for each spectrum was a clean ZnSe prism. The samples were hydrated by introducing an excess of deuterium oxide (^2H_2O) into a chamber placed on top of the ZnSe prism in the ATR casting and incubating for 5 min before acquiring the spectra. Hydrogen/deuterium exchange was considered complete because of the complete shift of the amide II band. Any contribution of ^2H_2O vapor to the absorbance spectra near the amide I peak region was eliminated by subtracting the spectra of pure lipids equilibrated with ^2H_2O under the same conditions.

ATR−FTIR Data Analysis. To resolve overlapping bands, we processed spectra using PEAKFIT (Jandel Scientific, San Rafael, CA) software. Fourth-derivative spectra were calculated to identify the positions of the component bands in the spectra. These wavenumbers were used as initial parameters for curve fitting with Gaussian component peaks. Positions, bandwidths, and amplitudes of the peaks were varied until a good agreement between the calculated sum of all components and the experimental spectra was achieved ($r^2 > 0.997$) under the following constraints: (i) the resulting bands shifted by no more than 2 cm^{-1} from the initial parameters, and (ii) all of the peaks had reasonable half-widths (<20–25 cm^{-1}). The relative amounts of the different secondary-structure elements were estimated by dividing the areas of individual peaks assigned to a particular secondary structure by the whole area of the resulting amide I band (*43*).

Preparation of Large Unilamellar Vesicles (LUVs). Thin films of PC were generated after dissolving the lipids in a 2:1 (v/v) mixture of $CHCL_3$/MeOH and drying them under a stream of nitrogen gas while rotating them. The films were lyophilized overnight, sealed with argon gas to prevent oxidation of the lipids, and stored at −20 °C. Before the experiments, films were suspended in the appropriate buffer and vortexed for 1.5 min. The lipid suspension underwent five cycles of freezing−thawing and extrusion through polycarbonate membranes with 1 and 0.1 μm diameter pores to create LUVs.

Fluorescence Measurements of NBD-Labeled Peptides. The fluorescence experiments were performed using NBD-labeled peptides. Fluorescence spectra were obtained at room temperature, with excitation set at 467 nm (10 nm slit) and emission scan at 500–600 nm (10 nm slits). In a typical experiment, a NBD-labeled peptide was added first from a stock solution in DMSO [final concentration of 0.5 μM and a maximum of 0.25% (v/v) DMSO] to a dispersion of PC LUV (100 μM) in PBS. This was followed by the addition of unlabeled CP in several sequential doses ranging from 0.125 to 1.5 μM (stock in DMSO). Fluorescence spectra were obtained before and after the addition of CP. The fluorescence values were corrected by subtracting the corresponding blank (buffer with the same vesicle concentration).

T-Cell Activation and Proliferation. T-cells were plated onto round 96-well plates in medium containing RPMI-1640 supplemented with 2.5% fetal calf serum (FCS), 100 units/mL penicillin, 100 μg/mL streptomycin, 50 μM 2β-mercaptoethanol, and 2 mM L-glutamine. We used 12×10^4 cells of the T-cell line specific to MOG p35-55, 5×10^5 irradiated (3000 rad) spleen cells (APC), and 10 μg/mL of MOG p35-55 were added to each well. In addition, different fusion peptide derivatives were added. Each determination was made at least in triplicate.

For some experiments, T cells were activated with immobilized anti-CD3 antibodies. After 72 h, at 37 °C in a 7.5% CO_2 humidified atmosphere, the T-cells were pulsed with 1 μCi (H^3) thymidine, with a specific activity of 5.0 Ci/mmol, for 7 h, and (H (*3*)) thymidine incorporation was measured using a 96-well plate β counter. The mean counts per minute (cpm) ± standard error was calculated for each triplicate or quadruplicate. The results of T-cell proliferation experiments are shown as the percentage of T-cell proliferation inhibition triggered by the antigen in the absence of FP.

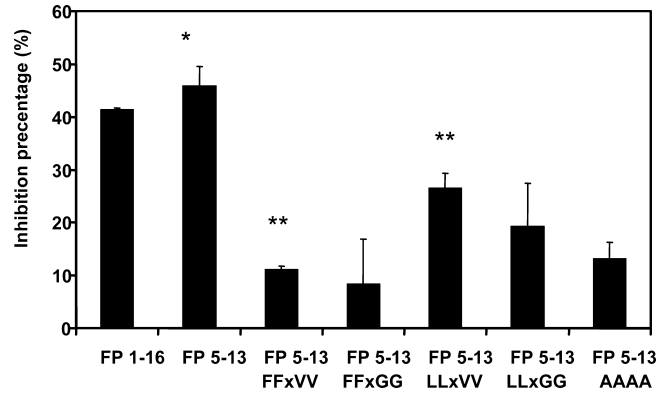

FIGURE 2: Inhibition of T-cell proliferation by the peptides. T-cells were activated with the MOG 35-55 peptide and APC in the presence of $FP_{5–13}$ and its derivatives (25 μg/mL), and the proliferative responses were assayed. The data are presented as mean inhibitions + SE ($n = 3$ or more). The uninhibited T-cell proliferative responses were 14301 ± 430 cpm. The background proliferation in the absence of antigen was 213 ± 44 cpm. (*) Inhibitory percentage of $FP_{5–13}$ was significantly more than any derivative ($p < 0.05$). (**) Inhibitory percentage of $FP_{5–13}$ LLxVV was significantly higher than the $FP_{5–13}$ FFxVV derivative ($p < 0.05$).

Mice. C57BL/6J mice were purchased from Harlan Olac (Bicester, U.K.). The mice were maintained in a specific pathogen-free facility and were used according to the guidelines and under the supervision of the animal welfare committee.

RESULTS

$FP_{5–13}$ Inhibits T-Cell Proliferation in Vitro. Recently, we have shown, using molecular dynamic simulation of the TCRα−TM/FP complex, that the $FP_{5–13}$ region is the interacting motif that binds to the TCRα−TM domain and interferes with T-cell activation (*23*). To investigate the underlying parameters within $FP_{5–13}$ responsible for this interaction, we synthesized a series of $FP_{5–13}$ amino-acid-substituted analogues (Table 1). In the first set of analogues, we replaced the two phenylalanines at positions 8 and 10 or the two leucines at positions 9 and 12 with the small-sized and nonhydrophobic amino acid glycine (designated $FP_{5–13}$ FFxGG and $FP_{5–13}$ LLxGG, respectively). In the second series of derivatives, we substituted the same amino acids with the hydrophobic amino acid valine (designated $FP_{5–13}$ FFxVV and $FP_{5–13}$ LLxVV, respectively). We then incubated each peptide in the presence of MOG p35–55 antigen with a T-cell line that is specific to MOG p35-55 and determined their proliferative response to the peptides after 3 days of incubation, using a H^3-thymidine uptake assay. MOG p35-55 is known to induce strong proliferative responses and cytokine release from this specific T-cell line. Figure 2 shows the inhibiting percentage caused by $FP_{5–13}$ and its amino-acid-substituted analogues. $FP_{5–13}$ inhibits ~45% T-cell proliferation response *in vitro*. However, practically no activity was observed when the two Phe residues were substituted, whereas substitution of Leu caused a less dramatic loss of activity. The $FP_{5–13}$ derivative, in which both Phe and Leu were replaced with alanine ($FP_{5–13}$ AAAA), was used as a negative control, because we replaced the entire motif and found very low/basal inhibitory activity.

The inhibitory effects of $FP_{5–13}$ and its analogues on antigen-triggered proliferation was not due to cell death,

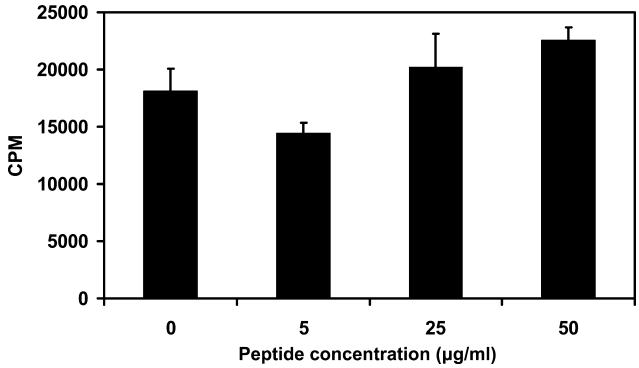

FIGURE 3: Noninhibitory effect of $FP_{5–13}$ toward T-cell activation induced by antibodies to CD3. T-cells were activated with 1 μg/mL anti-CD3 and APC in the presence of different $FP_{5–13}$ concentrations, and the proliferative responses were assayed.

because cells incubated with $FP_{5–13}$ and its derivatives, or a control, in which PBS was added, showed the same survival in culture (data not shown).

$FP_{5–13}$ Does Not Inhibit T-Cell Activation Induced by Antibodies to CD3. To determine whether $FP_{5–13}$ can also inhibit T-cell activation other than that induced by APC presentation of specific antigen, we tested the effect of $FP_{5–13}$ on T-cell activation induced by a mitogenic monoclonal antibody to CD3. $FP_{5–13}$, similar to the full-length $FP_{1–33}$ (*18*), did not inhibit the activation of T-cells by mitogenic anti-CD3 (Figure 3). Mitogenic anti-CD3 antibodies activate CD3 signaling regardless of the presence or absence of TCR (*44*). These findings support our assumption that $FP_{5–13}$ inhibits T-cell activation by interfering with TCR/CD3 crosstalk similarly to the full-length $FP_{1–33}$.

Changes in the Environment of $FP_{5–13}$ and Its Derivatives upon the Addition of CP Correlate with Biological Activity. NBD moiety can facilitate the determination of the environment of a NBD-labeled peptide in its membrane-bound state, because NBD fluorescence intensity is sensitive to the dielectric constant of its surroundings. This probe has already been used in many polarity and binding experiments (*2, 45, 46*). The fluorescence emission spectra of the NBD-labeled $FP_{5–13}$ and its derivatives were measured in the presence of PC LUV alone and in the presence of several sequential doses of unlabeled CP ranging from 0.125 to 1.5 μM. All NBD-labeled peptides exhibited very low-fluorescence signals in the presence of PC LUV alone. However, when the unlabeled CP was added, the fluorescence emission maxima of NBD−$FP_{5–13}$ increased sharply, concomitant with a blue shift (Figure 4A) A significant increase in the fluorescence of NBD was also observed with NBD−$FP_{5–13}$ LLxVV and NBD−$FP_{5–13}$ LLxGG (parts E and F of Figure 4 and Table 2.) Note that these three peptides could significantly inhibit T-cell proliferation. The other derivatives did not exhibit significant changes in their fluorescence intensity upon the addition of CP (parts B−D of Figure 4 and Table 2). These results indicate that $FP_{5–13}$ specifically recognizes CP, and because of this interaction, FP changes its environment probably by penetrating into the lipidic environment of the membrane.

Structure of the Peptides in Phospholipid Membranes Determined Using FTIR Spectroscopy. The FTIR spectra of $FP_{1–16}$ and $FP_{5–13}$ and its derivatives in PC multibilayers are shown in Figure 5. $FP_{1–16}$ and $FP_{5–13}$ have similar spectra with major peak (∼75%) characteristics of a β-sheet structure (parts G and A of Figure 5, respectively). In comparison, all of the analogues showed multipeak spectra, in which the percentages of the β-sheet structures are 40, 31, 16, 17, and 25%, for $FP_{5–13}$ LLxVV, $FP_{5–13}$ LLxGG, $FP_{5–13}$ FFxVV, $FP_{5–13}$ FFxGG, and $FP_{5–13}$ AAAA, respectively. These data reveal that the extent of the β-sheet component in the structure of the peptides correlates with the ability of the peptides to inhibit T-cell proliferation.

DISCUSSION

The data presented in this study strongly support the notion that the HIV-1 $FP_{5–13}$ region is the FP/TCRα-interacting motif. Its ability to inhibit T-cell proliferation in response to specific antigen is similar to that of the entire 16-mer fusion peptide. To understand the underlying parameters allowing this specific interaction, we synthesized and functionally and structurally analyzed a series of mutants derived from $FP_{5–13}$. The data reveal two interesting findings that relate to this interaction: (i) the β-sheet structure is a biologically active structure; several studies have shown that a similar structure was implicated in its membrane fusion activity, and (ii) the interaction between FP and TCRα−TM causes an insertion of the N terminus of $FP_{5–13}$ and its biologically active analogues into the membrane.

β-Sheet Structure Is the Biologically Active Conformation of FP upon Its Binding to the TCRα−TM Domain. The FTIR studies (Figure 5) suggest that $FP_{5–13}$ needs to adopt a β-sheet conformation to interact with CP to exert immunosuppressive activity. In support of this, the data reveal that the order of the increased β-sheet structure of the peptides (Figure 5) correlates with the order of their increased potential to inhibit T-cell proliferation: $FP_{5–13}$ > $FP_{5–13}$ LLxVV > $FP_{5–13}$ LLxGG > $FP_{5–13}$ FFxVV ≈ $FP_{5–13}$ FFxGG ≈ $FP_{5–13}$ AAAA. The importance of the β-sheet structure for exerting biological activity is in agreement with the molecular dynamic simulations of the interaction between the entire FP and the TCRα−TM domain (*23*). It is important to mention that previous structural characterization of the FP has revealed seemingly paradoxical data: α helix or β structure (*3, 6, 8, 9, 14, 24–39*). As indicated before, this apparent dichotomy may be explained by structural plasticity inherent in the FP based on its primary sequence given in Figure 1 (highly enriched in Gly and Ala). During the fusion event, both structures may be relevant and serve specific purposes.

In addition, the present data revealed a difference between the analogues in which the phenylalanines were replaced and those in which the leucines were replaced. In general, in comparison to the leucine-substituted analogues, substitution of the phenylalanines reduced the β-sheet component more (Figure 5), decreased the ability of the peptide to interact with CP (Figure 4), and inhibited T-cell proliferation (Figure 2). A possible explanation is that phenylalanine could create π−π aromatic interactions. Such interactions are highly important in the protein stabilization and assembly processes outside the membrane (*47, 48*). In addition, recent reports showed that aromatic residues are involved in the dimerization of TM domains of membrane proteins and that the aromatic motif, aromatic−X−X−aromatic, contributes, although partially to specificity, in TM domain assembly (*49*). In support of this, molecular dynamic simulation of the interaction between CP

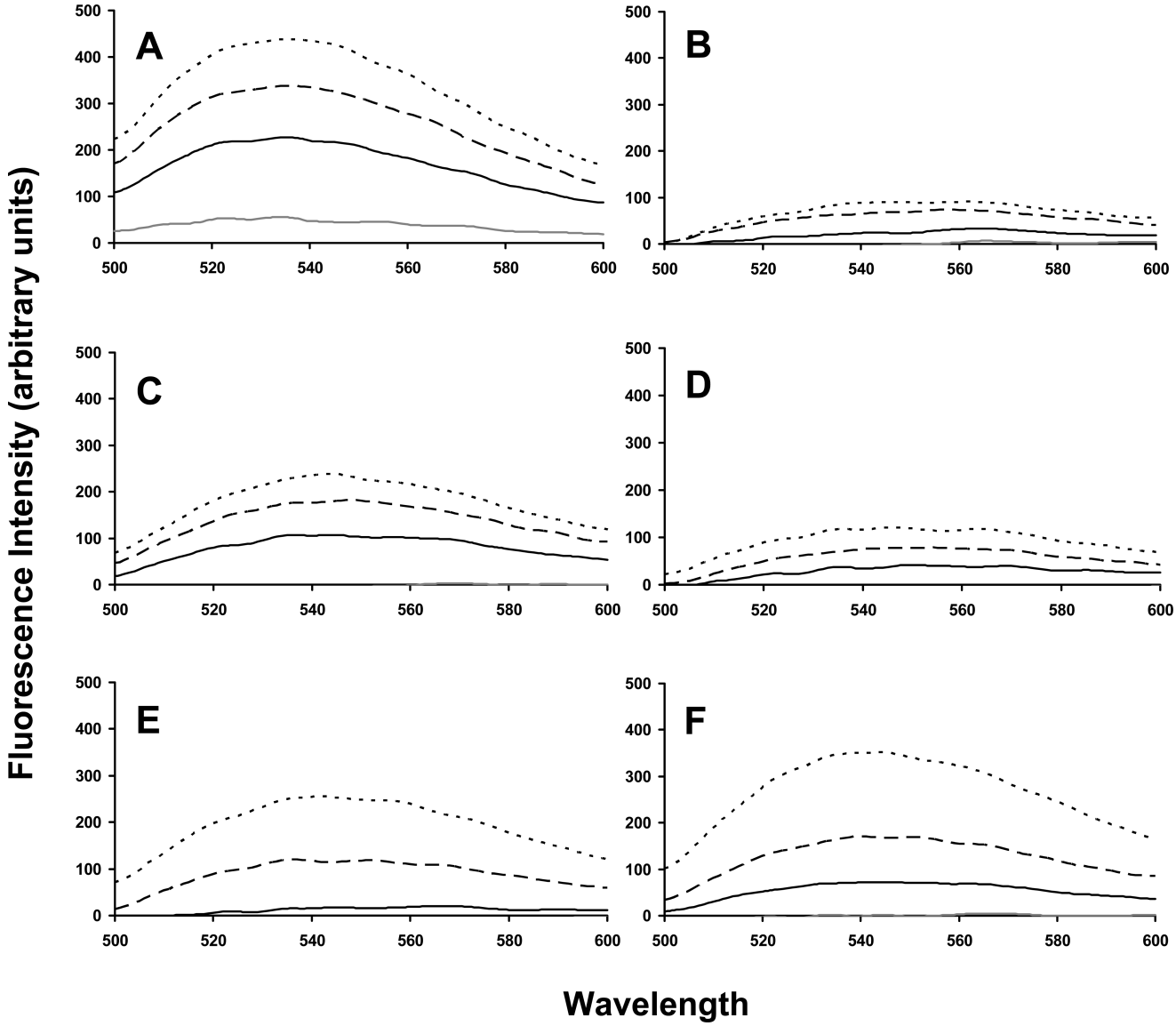

FIGURE 4: Changes in the environment of membrane-bound NBD-labeled $FP_{5–13}$ and its derivatives upon the addition of CP. The fluorescence experiments were performed using NBD-labeled $FP_{5–13}$ and its derivatives. Fluorescence spectra were obtained at room temperature, with excitation set at 467 nm (10 nm slit) and an emission scan at 500–600 nm (10 nm slits). In a typical experiment, a NBD-labeled peptide was added first to a dispersion of PC LUV (100 μM) in PBS. This was followed by the addition of an unlabeled CP peptide in several sequential doses. Fluorescence spectra were obtained in three different NBD-labeled peptides/CP ratio ranging from 1:0 to 1:3 (from the bottom to the top). NBD−$FP_{5–13}$ and NBD−$FP_{5–13}$ LLxVV (A and F, respectively) exhibited blue shifts concomitant with an increase in their fluorescence intensities around 530 nm, which indicates an environmental change of the labeled peptide. On the other hand, the other derivatives, $FP_{5–13}$ AAAA, $FP_{5–13}$ FFxGG, $FP_{5–13}$ FFxVV, and $FP_{5–13}$ LLxGG (B, C, D, and E, respectively), did not exhibit significant changes in their fluorescence intensity.

Table 2: Changes in the Environment of Membrane-Bound NBD-Labeled FP5-13 and Its Derivatives upon the Addition of CP[a]

$FP_{5–13}$ LLxVV	$FP_{5–13}$ LLxGG	$FP_{5–13}$ FFxVV	$FP_{5–13}$ FFxGG	$FP_{5–13}$ AAAA	$FP_{5–13}$	peptides ratio
0	0	0	0	0	54	1:0
70	15	37	106	21	227	1:1
165	119	70	175	61	337	1:2
347	250	116	228	85	437	1:3

[a] Fluorescence spectra were obtained at room temperature, with excitation set at 467 nm (10 nm slit) and the emission values at ~535 nm. Fluorescence spectra were obtained in three different NBD-labeled peptides/CP ratio ranging from 1:0 to 1:3.

and $FP_{1–16}$ resulted in an interaction between the phenylalanines from both regions (*23*). Note also that aromatic interactions play a role and act as a driving force in the creation of a β-sheet structure (*50*). Moreover, the gp41 protein forms trimers on the viral membrane (*51*), and FP itself oligomerizes in solution and in membranes (*10, 37*). It is therefore likely that phenylalanines and leucines are also required for this assembly, and therefore, the inhibitory effect of the peptides depends upon not only the interaction between FP and CP but also the interaction between several FP fragments needed for the assembly. The fusion peptide domain of the gp41 protein, which is highly conserved despite the frequent mutation of HIV-1 (*52, 53*), seems to be selected for its ability to inhibit T-cell proliferation.

Interaction Between CP and FP Moves the N-Terminal of CP toward the Hydrophobic Core of the Membrane. We labeled the N terminus of $FP_{5–13}$ and its analogues with NBD, let them interact with PC membranes, and followed their fluorescence upon the addition of CP. The data revealed that

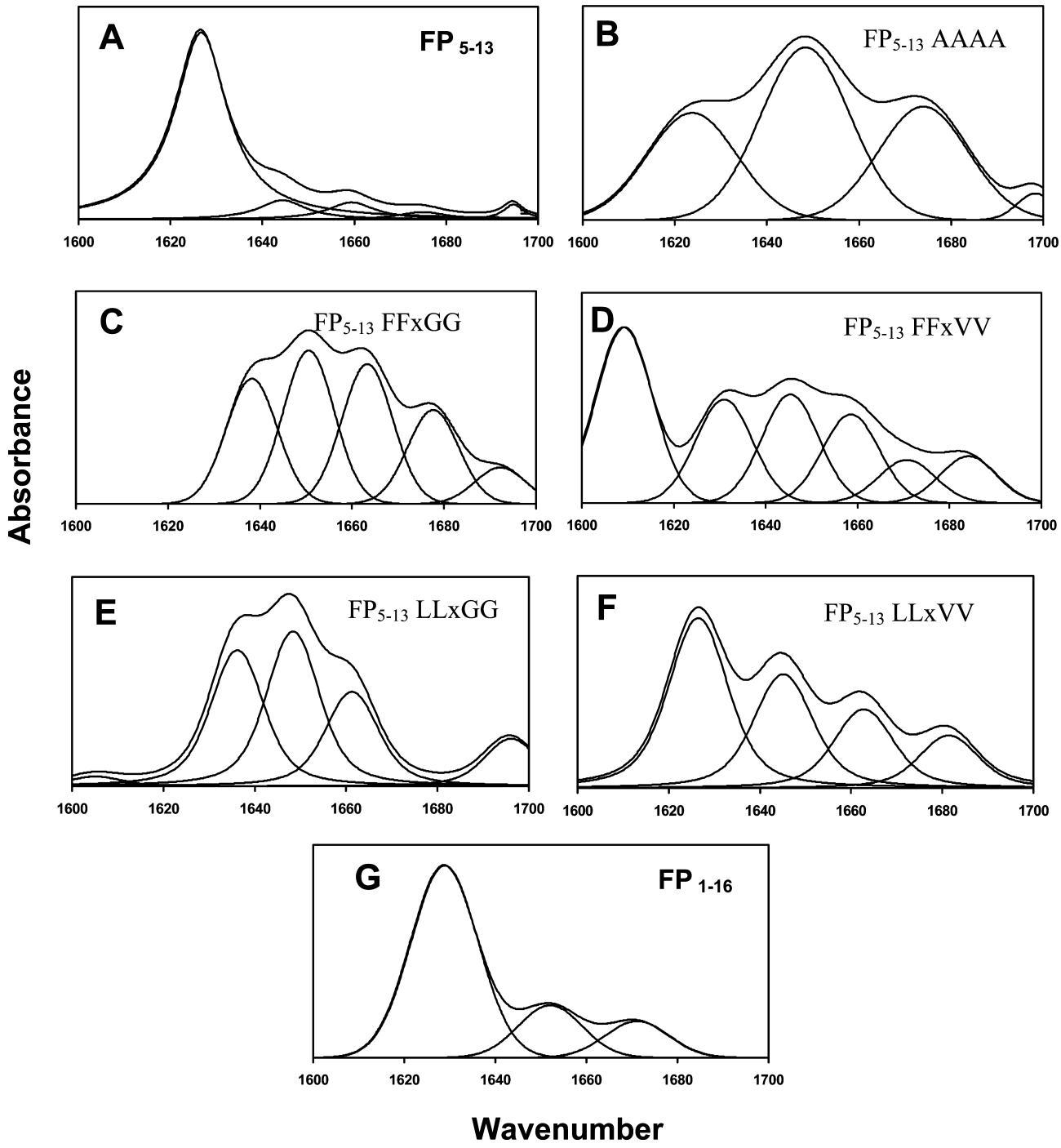

FIGURE 5: ATR−FTIR spectra of deuterated amide I band (1600–1700 cm^{-1}). FTIR spectra deconvolution of the fully deuterated amide I band (1600−1700 cm^{-1}) of peptides in PC multibilayers. Second derivatives were calculated to identify the positions of the component bands in the spectra. The component peaks result from curve fitting using a Gaussian line shape. The sums of the fitted components are superimposed on the experimental amide I region spectra. Upper curves represent the experimental FTIR spectra, and lower curves represent the fitted components. Designations of peptides are indicated in each panel of the figure. ATR−FTIR spectra deconvolution showing a clear β-sheet structure (∼75%) to $FP_{5–13}$ and $FP_{1–16}$ (A and G, respectively). Losses of β-sheet structure appear upon mutation within the $FP_{5–13}$ motif as shown in the ATR−FTIR spectra of $FP_{5–13}$ derivatives: B, $FP_{5–13}$ AAAA (∼25%); C, $FP_{5–13}$ FFxGG (∼17%); D, $FP_{5–13}$ FFxVV (∼16%); E, $FP_{5–13}$ LLxGG (∼31%), and F, $FP_{5–13}$ LLxVV (∼40%).

the interaction between CP and $FP_{5–13}$ caused a change in the location of the N-terminal of $FP_{5–13}$ to a more hydrophobic environment, as indicated by the marked increase in the fluorescence of the NBD group (Figure 4 and Table 2). These data suggest that the binding of CP to $FP_{5–13}$ caused most likely conformational changes resulting in its insertion into the hydrophobic core of the membrane. It is reasonable to assume that this conformational change allows for the creation of hydrogen bonds between the TCRα polar residues and the carbonyl atoms of the FP backbone that further stabilized the FP/TCRα complex inside the membrane (*23*). However, this model does not completely satisfy the energetic requirements of the hydrogen donor/acceptor atoms of the backbone between α helix and the single β strand inside the membrane. Nevertheless, the gp41 protein forms trimers (*51*) on the viral membrane, and FP itself oligomerizes in solution (*10, 37*). This allows FP to adopt a β-sheet conformation and still satisfy the energy requirement for

hydrogen bonds that would stabilize its interaction with α-helix CP. Despite the fact that such interactions are unusual, they might be favored by the special features of intermolecular interactions within the membrane milieu (*54, 55*).

Similar experiments were performed with all of the analogues. Importantly, the extent of the increase in fluorescence (Figure 4 and Table 2) correlates with the increase in the β-sheet structure of the different peptides (Figure 5), as well as with their ability to inhibit T-cell proliferation (Figure 2). However, we cannot rule out the possibility that the environment of the NBD moiety is also affected by a direct interaction with CP, which causes an intermolecular organization of the membrane-bound peptide. In both cases, the change in fluorescence indicates an interaction between CP and the corresponding FP analogues.

In summary, our data suggest that $FP_{5–13}$ needs to adopt a β-sheet conformation for efficient interaction with CP to induce immunosuppressive activity. Furthermore, the drastic loss of the $FP_{5–13}$ activity can explain why it is highly conserved within the different HIV strains; this supports its highly specific interaction with the CP region.

ACKNOWLEDGMENT

Y.S. holds the Harold S. and Harriet B. Brady Professorial Chair in Cancer Research. I.R.C. is the Mauerberger Professor of Immunology at the Weizmann Institute of Science and the director of the Center for the Study of Emerging Diseases, Jerusalem.

REFERENCES

1. Freed, E. O., Myers, D. J., and Risser, R. (1990) Characterization of the fusion domain of the human immunodeficiency virus type 1 envelope glycoprotein gp41. *Proc. Natl. Acad. Sci. U.S.A. 87*, 4650–4654.
2. Frey, S., and Tamm, L. K. (1990) Membrane insertion and lateral diffusion of fluorescence-labelled cytochrome *c* oxidase subunit IV signal peptide in charged and uncharged phospholipid bilayers. *Biochem. J. 272*, 713–719.
3. Gordon, L. M., Curtain, C. C., Zhong, Y. C., Kirkpatrick, A., Mobley, P. W., and Waring, A. J. (1992) The amino-terminal peptide of HIV-1 glycoprotein 41 interacts with human erythrocyte membranes: Peptide conformation, orientation and aggregation. *Biochim. Biophys. Acta 1139*, 257–274.
4. White, J. M. (1992) Membrane fusion. *Science 258*, 917–924.
5. Chan, D. C., Fass, D., Berger, J. M., and Kim, P. S. (1997) Core structure of gp41 from the HIV envelope glycoprotein. *Cell 89*, 263–273.
6. Rafalski, M., Lear, J. D., and DeGrado, W. F. (1990) Phospholipid interactions of synthetic peptides representing the N-terminus of HIV gp41. *Biochemistry 29*, 7917–7922.
7. Slepushkin, V. A., Andreev, S. M., Sidorova, M. V., Melikyan, G. B., Grigoriev, V. B., Chumakov, V. M., Grinfeldt, A. E., Manukyan, R. A., and Karamov, E. V. (1992) Investigation of human immunodeficiency virus fusion peptides. Analysis of interrelations between their structure and function. *AIDS Res. Hum. Retroviruses 8*, 9–18.
8. Martin, I., Defrise-Quertain, F., Decroly, E., Vandenbranden, M., Brasseur, R., and Ruysschaert, J. M. (1993) Orientation and structure of the NH2-terminal HIV-1 gp41 peptide in fused and aggregated liposomes. *Biochim. Biophys. Acta 1145*, 124–133.
9. Nieva, J. L., Nir, S., Muga, A., Goni, F. M., and Wilschut, J. (1994) Interaction of the HIV-1 fusion peptide with phospholipid vesicles: Different structural requirements for fusion and leakage. *Biochemistry 33*, 3201–3209.
10. Kliger, Y., Aharoni, A., Rapaport, D., Jones, P., Blumenthal, R., and Shai, Y. (1997) Fusion peptides derived from the HIV type 1 glycoprotein 41 associate within phospholipid membranes and inhibit cell−cell fusion. Structure−function study. *J. Biol. Chem. 272*, 13496–13505.
11. Blumenthal, R., Schoch, C., Puri, A., and Clague, M. J. (1991) A dissection of steps leading to viral envelope protein-mediated membrane fusion. *Ann. N.Y. Acad. Sci. 635*, 285–296.
12. Suarez, T., Nir, S., Goni, F. M., Saez-Cirion, A., and Nieva, J. L. (2000) The pre-transmembrane region of the human immunodeficiency virus type-1 glycoprotein: A novel fusogenic sequence. *FEBS. Lett. 477*, 145–149.
13. Epand, R. M. (2003) Fusion peptides and the mechanism of viral fusion. *Biochim. Biophys. Acta 1614*, 116–121.
14. Peisajovich, S. G., Epand, R. F., Pritsker, M., Shai, Y., and Epand, R. M. (2000) The polar region consecutive to the HIV fusion peptide participates in membrane fusion. *Biochemistry 39*, 1826–1833.
15. Poumbourios, P., Wilson, K. A., Center, R. J., El Ahmar, W., and Kemp, B. E. (1997) Human immunodeficiency virus type 1 envelope glycoprotein oligomerization requires the gp41 amphipathic α-helical/leucine zipper-like sequence. *J. Virol. 71*, 2041–2049.
16. Weissenhorn, W., Dessen, A., Calder, L. J., Harrison, S. C., Skehel, J. J., and Wiley, D. C. (1999) Structural basis for membrane fusion by enveloped viruses. *Mol. Membr. Biol. 16*, 3–9.
17. Peisajovich, S. G., and Shai, Y. (2003) Viral fusion proteins: Multiple regions contribute to membrane fusion. *Biochim. Biophys. Acta 1614*, 122–129.
18. Quintana, F. J., Gerber, D., Kent, S. C., Cohen, I. R., and Shai, Y. (2005) HIV-1 fusion peptide targets the TCR and inhibits antigen-specific T cell activation. *J. Clin. Invest. 115*, 2149–2158.
19. Freed, E. O., Delwart, E. L., Buchschacher, G. L., Jr., and Panganiban, A. T. (1992) A mutation in the human immunodeficiency virus type 1 transmembrane glycoprotein gp41 dominantly interferes with fusion and infectivity. *Proc. Natl. Acad. Sci. U.S.A. 89*, 70–74.
20. Weissenhorn, W., Dessen, A., Harrison, S. C., Skehel, J. J., and Wiley, D. C. (1997) Atomic structure of the ectodomain from HIV-1 gp41. *Nature 387*, 426–430.
21. Kliger, Y., Peisajovich, S. G., Blumenthal, R., and Shai, Y. (2000) Membrane-induced conformational change during the activation of HIV-1 gp41. *J. Mol. Biol. 301*, 905–914.
22. Kliger, Y., Gallo, S. A., Peisajovich, S. G., Munoz-Barroso, I., Avkin, S., Blumenthal, R., and Shai, Y. (2001) Mode of action of an antiviral peptide from HIV-1. Inhibition at a post-lipid mixing stage. *J. Biol. Chem. 276*, 1391–1397.
23. Bloch, I., Quintana, F. J., Gerber, D., Cohen, T., Cohen, I. R., and Shai, Y. (2007) T-cell inactivation and immunosuppressive activity induced by HIV gp41 via novel interacting motif. *FASEB J. 21*, 393–401.
24. Mobley, P. W., Waring, A. J., Sherman, M. A., and Gordon, L. M. (1999) Membrane interactions of the synthetic N-terminal peptide of HIV-1 gp41 and its structural analogs. *Biochim. Biophys. Acta 1418*, 1–18.
25. Martin, I., Schaal, H., Scheid, A., and Ruysschaert, J. M. (1996) Lipid membrane fusion induced by the human immunodeficiency virus type 1 gp41 N-terminal extremity is determined by its orientation in the lipid bilayer. *J. Virol. 70*, 298–304.
26. Gordon, L. M., Lee, K. Y., Lipp, M. M., Zasadzinski, J. A., Walther, F. J., Sherman, M. A., and Waring, A. J. (2000) Conformational mapping of the N-terminal segment of surfactant protein B in lipid using ^{13}C-enhanced Fourier transform infrared spectroscopy. *J. Pept. Res. 55*, 330–347.
27. Gordon, L. M., Mobley, P. W., Pilpa, R., Sherman, M. A., and Waring, A. J. (2002) Conformational mapping of the N-terminal peptide of HIV-1 gp41 in membrane environments using ^{13}C-enhanced Fourier transform infrared spectroscopy. *Biochim. Biophys. Acta 1559*, 96–120.
28. Gordon, L. M., Mobley, P. W., Lee, W., Eskandari, S., Kaznessis, Y. N., Sherman, M. A., and Waring, A. J. (2004) Conformational mapping of the N-terminal peptide of HIV-1 gp41 in lipid detergent and aqueous environments using ^{13}C-enhanced Fourier transform infrared spectroscopy. *Protein Sci. 13*, 1012–1030.
29. Pereira, F. B., Goni, F. M., Muga, A., and Nieva, J. L. (1997) Permeabilization and fusion of uncharged lipid vesicles induced by the HIV-1 fusion peptide adopting an extended conformation: Dose and sequence effects. *Biophys. J. 73*, 1977–1986.
30. Curtain, C., Separovic, F., Nielsen, K., Craik, D., Zhong, Y., and Kirkpatrick, A. (1999) The interactions of the N-terminal fusogenic peptide of HIV-1 gp41 with neutral phospholipids. *Eur. Biophys. J. 28*, 427–436.
31. Yang, J., Gabrys, C. M., and Weliky, D. P. (2001) Solid-state nuclear magnetic resonance evidence for an extended β strand

conformation of the membrane-bound HIV-1 fusion peptide. *Biochemistry 40*, 8126–8137.
32. Yang, R., Yang, J., and Weliky, D. P. (2003) Synthesis, enhanced fusogenicity, and solid state NMR measurements of cross-linked HIV-1 fusion peptides. *Biochemistry 42*, 3527–3535.
33. Yang, J., and Weliky, D. P. (2003) Solid-state nuclear magnetic resonance evidence for parallel and antiparallel strand arrangements in the membrane-associated HIV-1 fusion peptide. *Biochemistry 42*, 11879–11890.
34. Yang, R., Prorok, M., Castellino, F. J., and Weliky, D. P. (2004) A trimeric HIV-1 fusion peptide construct which does not self-associate in aqueous solution and which has 15-fold higher membrane fusion rate. *J. Am. Chem. Soc. 126*, 14722–14723.
35. Jaroniec, C. P., Kaufman, J. D., Stahl, S. J., Viard, M., Blumenthal, R., Wingfield, P. T., and Bax, A. (2005) Structure and dynamics of micelle-associated human immunodeficiency virus gp41 fusion domain. *Biochemistry 44*, 16167–16180.
36. Yang, J., Prorok, M., Castellino, F. J., and Weliky, D. P. (2004) Oligomeric β-structure of the membrane-bound HIV-1 fusion peptide formed from soluble monomers. *Biophys. J. 87*, 1951–1963.
37. Sackett, K., and Shai, Y. (2005) The HIV fusion peptide adopts intermolecular parallel β-sheet structure in membranes when stabilized by the adjacent N-terminal heptad repeat: A ^{13}C FTIR study. *J. Mol. Biol. 350*, 790–805.
38. Zheng, Z., Yang, R., Bodner, M. L., and Weliky, D. P. (2006) Conformational flexibility and strand arrangements of the membrane-associated HIV fusion peptide trimer probed by solid-state NMR spectroscopy. *Biochemistry 45*, 12960–12975.
39. Li, Y., and Tamm, L. K. (2007) Structure and plasticity of the human immunodeficiency virus gp41 fusion domain in lipid micelles and bilayers. *Biophys. J. 93*, 876–885.
40. Gerber, D., and Shai, Y. (2000) Insertion and organization within membranes of the δ-endotoxin pore-forming domain, helix 4−loop−helix 5, and inhibition of its activity by a mutant helix 4 peptide. *J. Biol. Chem. 275*, 23602–23607.
41. Gazit, E., Miller, I. R., Biggin, P. C., Sansom, M. S., and Shai, Y. (1996) Structure and orientation of the mammalian antibacterial peptide cecropin P1 within phospholipid membranes. *J. Mol. Biol. 258*, 860–870.
42. Surewicz, W. K., Mantsch, H. H., and Chapman, D. (1993) Determination of protein secondary structure by Fourier transform infrared spectroscopy: A critical assessment. *Biochemistry 32*, 389–394.
43. Jackson, M., and Mantsch, H. H. (1995) The use and misuse of FTIR spectroscopy in the determination of protein structure. *Crit. Rev. Biochem. Mol. Biol. 30*, 95–120.
44. Wang, X. M., Djordjevic, J. T., Kurosaka, N., Schibeci, S., Lee, L., Williamson, P., and Manolios, N. (2002) T-cell antigen receptor peptides inhibit signal transduction within the membrane bilayer. *Clin. Immunol. 105*, 199–207.
45. Rajarathnam, K., Hochman, J., Schindler, M., and Ferguson-Miller, S. (1989) Synthesis, location, and lateral mobility of fluorescently labeled ubiquinone 10 in mitochondrial and artificial membranes. *Biochemistry 28*, 3168–3176.
46. Rapaport, D., and Shai, Y. (1991) Interaction of fluorescently labeled pardaxin and its analogues with lipid bilayers. *J. Biol. Chem. 266*, 23769–23775.
47. Serrano, L., Bycroft, M., and Fersht, A. R. (1991) Aromatic−aromatic interactions and protein stability. Investigation by double-mutant cycles. *J. Mol. Biol. 218*, 465–475.
48. Burley, S. K., and Petsko, G. A. (1985) Aromatic−aromatic interaction: A mechanism of protein structure stabilization. *Science 229*, 23–28.
49. Sal-Man, N., Gerber, D., Bloch, I., and Shai, Y. (2007) Specificity in transmembrane helix−helix interactions mediated by aromatic residues. *J. Biol. Chem. 282*, 19753–19761.
50. Aggeli, A., Bell, M., Boden, N., Keen, J. N., Knowles, P. F., McLeish, T. C., Pitkeathly, M., and Radford, S. E. (1997) Responsive gels formed by the spontaneous self-assembly of peptides into polymeric β-sheet tapes. *Nature 386*, 259–262.
51. Center, R. J., Leapman, R. D., Lebowitz, J., Arthur, L. O., Earl, P. L., and Moss, B. (2002) Oligomeric structure of the human immunodeficiency virus type 1 envelope protein on the virion surface. *J. Virol. 76*, 7863–7867.
52. de Jong, M. D., Schuurman, R., Lange, J. M., and Boucher, C. A. (1996) Replication of a pre-existing resistant HIV-1 subpopulation in vivo after introduction of a strong selective drug pressure. *Antiviral Ther. 1*, 33–41.
53. Mayers, D. L. (1997) Prevalence and incidence of resistance to zidovudine and other antiretroviral drugs. *Am. J. Med. 102*, 70–75.
54. Fleming, K. G., and Engelman, D. M. (2001) Specificity in transmembrane helix−helix interactions can define a hierarchy of stability for sequence variants. *Proc. Natl. Acad. Sci. U.S.A. 98*, 14340–14344.
55. Senes, A., Ubarretxena-Belandia, I., and Engelman, D. M. (2001) The Cα—H···O hydrogen bond: A determinant of stability and specificity in transmembrane helix interactions. *Proc. Natl. Acad. Sci. U.S.A. 98*, 9056–9061.
56. Manolios, N., Collier, S., Taylor, J., Pollard, J., Harrison, L. C., and Bender, V. (1997) T-cell antigen receptor transmembrane peptides modulate T-cell function and T cell-mediated disease. *Nat. Med. 3*, 84–88.

BI800100P